molecular pharmaceutics

Article

pubs.acs.org/molecularpharmaceutics

Flash Nanoprecipitation: Particle Structure and Stability

Kevin M. Pustulka,[†] Adam R. Wohl,[‡] Han Seung Lee,[†] Andrew R. Michel,[‡] Jing Han,[†] Thomas R. Hoye,[‡] Alon V. McCormick,[†] Jayanth Panyam,[§] and Christopher W. Macosko*,[†]

[†]Department of Chemical Engineering and Materials Science, [‡]Department of Chemistry, and [§]Department of Pharmaceutics, University of Minnesota, Minneapolis, Minnesota 55455, United States

ABSTRACT: Flash nanoprecipitation (FNP) is a process that, through rapid mixing, stabilizes an insoluble low molecular weight compound in a nanosized, polymer-stabilized delivery vehicle. The polymeric components are typically amphiphilic diblock copolymers (BCPs). In order to fully exploit the potential of FNP, factors affecting particle structure, size, and stability must be understood. Here we show that polymer type, hydrophobicity and crystallinity of the small molecule, and small molecule loading levels all affect particle size and stability. Of the four block copolymers (BCP) that we have studied here, poly(ethylene glycol)-*b*-poly(lactic-*co*-glycolic acid) (PEG-*b*-PLGA) was most suitable for potential drug delivery applications due to its ability to give rise to stable nanoparticles, its biocompatibility, and its degradability. We found little difference in particle size when using PLGA block sizes over the range of 5 to 15 kDa. The choice of hydrophobic small molecule was important, as molecules with a calculated water−octanol partition coefficient (clogP) below 6 gave rise to particles that were unstable and underwent rapid Ostwald ripening. Studies probing the internal structure of nanoparticles were also performed. Analysis of differential scanning calorimetry (DSC), cryogenic transmission electron microscopy (cryo-TEM), and ^{1}H NMR experiments support a three-layer core−shell−corona nanoparticle structure.

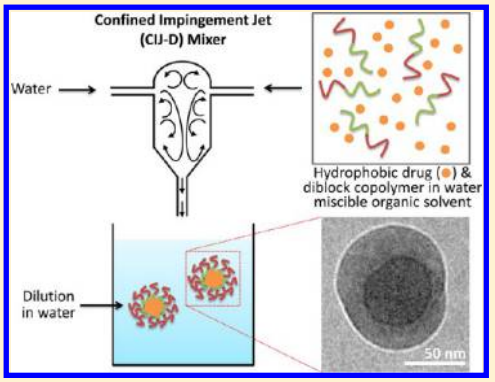

KEYWORDS: *flash nanoprecipitation, insoluble drugs, drug delivery, paclitaxel, core−shell particles*

1. INTRODUCTION

Approximately 30−40% of new drug candidates have poor aqueous solubility, presenting difficulties in developing suitable formulations.[1] Nanoscale carriers show great promise for the delivery of hydrophobic drugs and can be further designed to positively affect the biodistribution of the encapsulated drug .[2] The nanometer size range enables longer systemic circulation by reducing renal clearance and by minimizing uptake by the reticuloendothelial system.[3] Nanoscale drug delivery systems are particularly important in cancer research due to their ability to exploit the abnormal tumor vasculature via the enhanced permeation and retention (EPR) effect.[4]

Most nano drug carrier systems including liposomes,[5] polymer vesicles,[6] and polymeric micelles[7,8] range in size from 50 to 400 nm. However, the typical drug loading capacity of these systems is low (typically less than 10%).[9−11] Formulations having higher drug loading levels offer the potential for more of the drug to localize in the desired tissue, resulting in lowered dosage to achieve the same therapeutic outcomes. In addition, more highly loaded delivery vehicles mean that less excipient can be used.[12] One way to produce such carriers is to efficiently entrap the drug compound in kinetically stabilized nanoparticles via the process of flash nanoprecipitation (FNP).

Flash nanoprecipitation (FNP) is a simple, scalable process using rapid micromixing to create high supersaturation conditions leading to the precipitation and encapsulation of hydrophobic drugs in a polymer based delivery vehicle. The process, developed by Prud'homme and co-workers,[13,14] uses either a four stream multi inlet vortex (MIV) mixer[15] or a two stream confined impingement jet mixer with subsequent dilution (CIJ-D).[16] In both cases, the organic solutes (i.e., drug) and amphiphilic block copolymers (BCPs) are dissolved in a water miscible organic solvent. Rapid (and turbulent) mixing of the organic solvent stream with water induces supersaturation, which initiates precipitation of the dissolved hydrophobic components. Prud'homme et al.[13−15] proposed that the hydrophobic block of the BCP and the hydrophobic drug are encapsulated in the core of the nanoparticle. The hydrophilic block forms a corona, sterically stabilizing the particles by preventing further aggregation. Accordingly, otherwise insoluble compounds can be stably dispersed in an aqueous environment. The process of preparing nanoparticles by FNP using the MIV or the CIJ-D mixer is illustrated in Figure 1.

Many different BCPs have been used to stabilize nanoparticles in FNP.[13,17−22,25,27,28] FNP has been used to produce nanoparticles of a wide variety of hydrophobic molecules: bifenthrin,[22] paclitaxel prodrugs,[23−25] β-carotene,[13,14,26,27] vitamin E,[21,25] nitric oxide prodrugs,[28] hydrophobic fluorophores,[21] nanophosphors,[29] curcumin,[30] and even sunscreen

Received: August 4, 2013
Revised: September 14, 2013
Accepted: September 20, 2013
Published: September 20, 2013

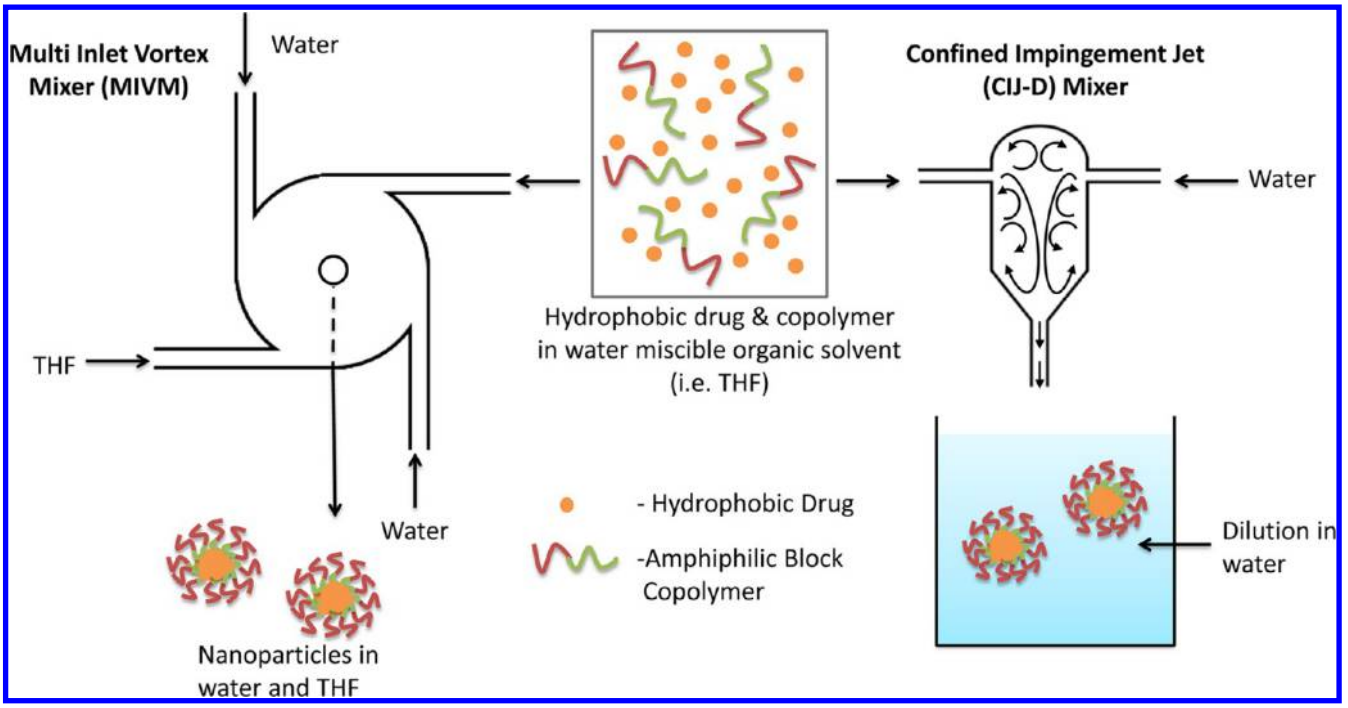

Figure 1. Schematic diagram of the multi inlet vortex (MIV) mixer and the confined impingement jet (CIJ-D)[16] mixer. In either, the final concentration of organic solvent is <10%. In the MIV mixer this is achieved by higher water flow rates and a correspondingly greater volume of the inlet water streams. In the CIJ-D there are only two inlets, so the flow must be of equal velocity to balance momentum. Dilution of the organic solvent is achieved by immediate injection into excess water. Depending upon exact flow rates, the residence time inside the mixing chamber is on the order of 10 ms.

agents.[31] However, to our knowledge there has been no comprehensive study on how the choice of BCP, solute, and their formulation conditions affects nanoparticle size and stability. Additionally, while the method of particle formation and thus particle structure has been hypothesized,[14,15,18,22] and studied via molecular modeling,[32] the internal nanoparticle structure has not yet been elucidated.

We report here the effect of formulation parameters in FNP on nanoparticle size and stability. The effect of type of BCP and compound as well as loading and concentration on nanoparticle formation was determined. In addition to studying the materials used to make nanoparticles, we have also carried electron microscopy studies aimed at achieving a better understanding of the nanoparticle structure.

2. EXPERIMENTAL SECTION

2.1. Materials. β-Carotene (≥97%), betulin (≥98%), curcumin (≥80%), triethylamine (TEA; ≥99.5%), octanoic acid (≥98%), silicon tetrachloride (99%), water (H_2O; HPLC grade), methanol (HPLC grade), dichloromethane (anhydrous; ≥99.8%), and tetrahydrofuran (THF; HPLC grade) were purchased from Aldrich. Triethoxychlorosilane (95%) was purchased from Gelest Incorporated. Acetone was purchased as ACS grade from Fischer chemical. Acetone-d_6 (D, 99.9%) and D_2O (D, 99.9%) were purchased from Cambridge Isotope Laboratories Incorporated. Paclitaxel was obtained from Phytogen Life Sciences. 2,4,6-Triiodophenol was obtained from Alfa Aesar (98% purity). Hydrocortisone was obtained from MP Biomedical (99.6% by HPLC, USP).

PS(10k)-*b*-PEG(5k) (M_w/M_n = 1.05) was purchased from Polymer Source. (D,L)-Lactide [or (*rac*)-lactide] was purchased from Altasorb and purified by recrystallization from toluene; glycolide was purchased from Altasorb and was purified by recrystallization from THF. Monomethoxy PEG (M_n = 2000 and 5000 g·mol^{-1}, denoted mPEG(2k or 5k)-OH), PEG-diol (HO-PEG(5k)-OH), monomethoxy diethylene glycol, ε-caprolactone 97%, (1*R*)-(−)-10-camphorsulfonic acid (98%), and 1,8-diazabicyclo[5.4.0]undec-7-ene were purchased from Aldrich, and mPEG(10k)-OH was purchased from JenKem Technology. Prior to its use in synthesizing mPEG-containing BCPs, mPEG-OH was dried by azeotropic distillation from toluene or by dissolution in dry dichloromethane and storage overnight on oven-dried molecular sieves in an airtight culture tube.

2.2. Polymer Synthesis. HO-PEG(5k)-*b*-PCL(12k) was synthesized by coupling acid chloride PCL (PCL-COCl) with an excess of dihydroxy-terminated PEG (HO-PEG(5k)-OH). PCL-COCl was prepared from carboxylic terminated PCL (PCL-COOH), which was synthesized by ring-opening transesterification polymerization of ε-caprolactone using octanoic acid as the initiator and camphorsulfonic acid as the catalyst. The BCP was then fractionated into different molecular weights by selective precipitation from THF/methanol cosolvent.[33] The M_n of each sample was determined by ^{1}H NMR spectroscopic analysis.

PEG-*b*-PLGA was made by a controlled ring-opening copolymerization of glycolide and lactide using mPEG-OH as the macroinitiator and 1,8-diazabicyclo[5.4.0]undec-7-ene (DBU) as the organic catalyst, as described by Qian et al.[34] PEG-*b*-PLA was also synthesized as described by Qian et al.[34] Both the PEG-*b*-PLGA and PEG-*b*-PLA M_ns were determined by ^{1}H NMR spectroscopic analysis. The number average molecular weight (M_n) of the PLGA and PLA blocks was calculated by comparison of the ratio of the integrations of the methine and methylene signal of the lactic and glycolic resonances against the methylene signal of the PEG backbone.

dx.doi.org/10.1021/mp400337f | *Mol. Pharmaceutics* 2013, 10, 4367−4377

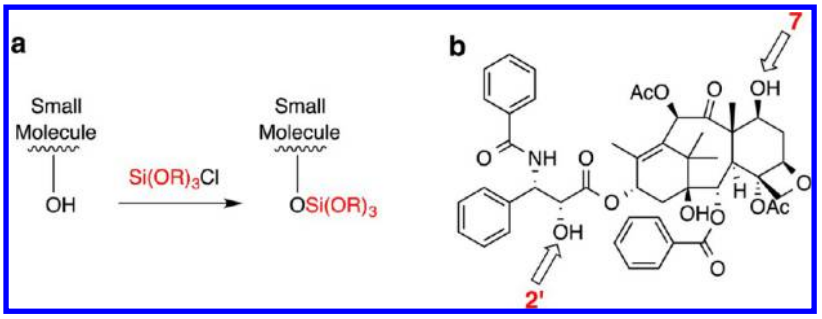

Figure 2. (a) Reaction scheme for the formation of silicate derivatives. Altering the nature of the alkyl moiety R allows the hydrophobicity of the derivative to be tuned. (b) Structure of paclitaxel showing the C2′ and C7 hydroxyl groups.

The manufacturer-reported molecular weight of the PEG was used as the reference value for deducing the relative sizes of the two blocks.

2.3. Paclitaxel Silicate Synthesis. Silicate derivatives of paclitaxel (PTX, Figure 2b) were synthesized as described by Wohl.[35] Figure 2a shows the general strategy: a chlorosilane was used to derivatize one or two of the hydroxyl groups (at C2′ and C7) on PTX to form the silicate derivatives. Altering the alkyl moiety R allows for the hydrophobicity to be tuned. PTX silicates were synthesized to include monosubstitution at the C2′ position and a bis-silylated silicate at both the C2′ and C7 positions. The compounds described in this study are shown in Table 3.

2.4. Particle Preparation. The following is a typical procedure for particle preparation using the MIV mixer.[18] Two of the four mixer inlets were connected to two gastight plastic syringes (60 mL, Kendall Monojet) via Teflon tubing (1.6 mm i.d.). Each syringe contained 45 mL of water and was driven into the mixer by an infusion syringe pump (Harvard Apparatus, model 945). The other two inlets were connected to two gastight glass syringes (10 mL, SGE) via Teflon tubing. One of these contained 5 mL of a THF solution with the dissolved hydrophobic small molecule and BCP (e.g., 50 mg of each component if a 50% load level was desired), while the other contained 5 mL of pure THF. The two glass syringes were driven by a second infusion syringe pump (Harvard Apparatus, PHD 2000 programmable). The pumps propelled the four streams at high velocity into the small mixing chamber (25 μL) generating high turbulence.[15] For most experiments, the flow rates were 120 mL/min for the 60 mL plastic syringes and 13.3 mL/min for the glass syringes containing the organic solutions. The final nanoparticle suspension was 0.1 wt % in 90:10 water:THF. Particles were also prepared with acetone, and similar results have been found with slightly smaller particle sizes. However, acetone was ultimately not used due to the instability of nanoparticles prepared with high drug loading.

The following is a typical procedure for particle preparation using the CIJ-D mixer. For the organic stream, 25 mg of a hydrophobic small molecule and 25 mg of an amphiphilic BCP were dissolved in 2.5 mL of an organic solvent (e.g., THF). This solution was then placed in a 3 mL plastic syringe. A second syringe (3 mL) was loaded with 2.5 mL of deionized water. These two syringes were attached to the two vertical openings on the CIJ-D mixer.[16] A beaker containing 45.0 mL of deionized water was placed at the exit of the mixer. The exit stream outlet was submerged in water. The two syringes were then pushed rapidly and simultaneously by hand to inject the liquids into the CIJ-D mixer at equal rates, where the two streams rapidly mixed. This process produced a 0.1 wt % nanoparticle suspension in a 95:5 water:THF

2.5. Nanoparticle Characterization. Nanoparticle size was determined by dynamic light scattering (DLS) using a ZetaPALS (Brookhaven Instruments, diode laser BI-DPSS wavelength of 659 nm). For each sample, 3 separate DLS cuvettes were prepared and the hydrodynamic diameter was measured. The reported diameter is the average of the three separate runs. All values are hydrodynamic diameters calculated by the instrument software.

Scanning electron microscopy (SEM) was used to characterize the morphology and size of some samples of nanoparticles following the procedure described by Zhu.[18] Samples were prepared by first filling a glass Pasteur pipet with the nanosuspension and then emptying it, leaving small droplets inside the pipet. These were then aspirated onto a silica wafer that had been washed with HPLC grade THF and water. After evaporation of the solvent at room temperature, the sample was sputter coated with a 30 Å layer of platinum and imaged using a JEOL 6500 SEM.

X-ray diffraction was used to determine the crystallinity of the small molecule encapsulated in nanoparticles. The XRD pattern was collected on a PANalytical X′Pert Pro MPD diffractometer equipped with a cobalt anode (45 kV, 40 mA, λ = 1.790 Å) and an X-Celerator detector.

Transmission electron microscopy (TEM, FEI Tecnai T12) was also used to characterize the morphology and size of some of the nanoparticles. TEM grids (carbon type-B, 200 copper mesh, grid hole size of ~97 μm) and uranyl acetate were purchased from Ted Pella. Approximately 5 μL of the nanoparticle suspension was placed on the TEM grid. The extra suspension was then tapped off, leaving a thin film on the grid. A small drop of the 2 wt % uranyl acetate solution was then placed on the TEM grid and allowed to sit for 2−3 min before being wicked away from the underside of the grid with a piece of Whatman No.1 filter paper. The staining procedure was then repeated and the sample was allowed to dry before being analyzed by TEM.

Cryogenic transmission electron microscopy (cryo-TEM) samples were prepared with a FEI Vitrobot Mark III. Holey carbon grids (01881, 200 copper mesh, Ted Pella, Ltd.) were glow discharged in a Denton DV-502A vacuum evaporator at 70 mTorr to prepare a hydrophilic surface. 3 μL of sample was applied to the grids at 22 °C and 100% relative humidity. After the application, the samples were plunged into liquid ethane and vitrified.[36] The samples were then viewed in a 120 kV FEI Tecnai Spirit BioTWIN at −178 °C. The images were digitally recorded using a FEI Eagle 2k CCD camera in a low-dose

dx.doi.org/10.1021/mp400337f | Mol. Pharmaceutics 2013, 10, 4367−4377

mode and processed with FEI TEM Imaging and Analysis software package.

Differential scanning calorimetry (DSC) was performed using a TA Instruments Discovery DSC that was calibrated using high-purity indium and a heating rate of 10 °C/min. Typical sample size was 1 mg for polymer but only 0.2 mg for some of the dry nanoparticles due to their high electrostatic charge and low bulk density.

Diffusion oriented spectroscopy (DOSY) NMR measurements were performed on a 300 MHz Varian NMR spectrometer at ambient temperature. The 1D ^{1}H NMR experiment was performed first (number of transients = 16). The 90° pulse width was determined, and the 1D ^{1}H NMR experiment was repeated. Typical parameters obtained from the 1D experiment were pulse width = 17 ms, spectral width = 2007.3 Hz, transmitter offset −628.4 Hz, and gain = 50. These were then used for the DOSY experiment. A series of spectra were then obtained (with the diffusion time set to 0.03 s) such that the final signals decayed to approximately 10% of their original intensity. The spectra were baseline-corrected and processed using the Varian software.

3. RESULTS AND DISCUSSION

3.1. Choice of Block Copolymer. To better understand the role of the type of BCP used in FNP, we studied four relatively low molecular weight diblock copolymers. β-Carotene, a precursor of vitamin A, was used as a model drug in this study due to its high hydrophobicity. Previous studies have shown that nanoparticles with only β-carotene (without any added block copolymer) can be made using FNP.[16] These particles were stable, likely due to a small negative surface charge (ξ = −20 mV), but for only a few hours. To stabilize β-carotene nanoparticles, BCPs with four different hydrophobic blocks, each about 10 kDa in size, were used: 5k−10k PEG-*b*-PS, 5k−12k PEG-*b*-PCL, 5k−10k PEG-*b*-PLA, and 5k−10k PEG-*b*-PLGA. In each case, an equal mass of β-carotene and stabilizing BCP was used and particles were made using the MIV mixer. Zeta potential (ξ) was measured for all the particles; all were negatively charged at 10 to 30 mV depending on the block copolymer. Once saline was added, |ξ| decreased to near zero. This indicates that the nanoparticles were sterically stabilized by BCP, rather than electrostatically

Table 1. T_g and Solubility Parameter, δ, of β-Carotene and Polymer Block

	T_g (°C)	$\delta_{polymer}$ or δ_β (MPa$^{1/2}$)[a]	$\lvert\Delta\delta_{PEG}\rvert$[b] (MPa$^{1/2}$)	$\lvert\Delta\delta_\beta\rvert$ (MPa$^{1/2}$)
β-carotene		17.8	3.6	0
PEG (5k)	−60[43]	21.4	0	3.6
PS (10k)	101[44]	19.6	1.8	1.8
PCL (12k)	−60[45]	19.7	1.7	1.9
PLA (10k)	23[46]	21.3	0.1	3.5
PLGA (10k)	39[47,50]	22.5	1.1	4.7

[a]Hoy solubility parameter calculator: http://www.compchemcons.com. [b]$\lvert\Delta\delta_{PEG}\rvert = \lvert\delta_{polymer} - \delta_{PEG}\rvert$, $\lvert\Delta\delta_\beta\rvert = \lvert\delta_{polymer} - \delta_\beta\rvert$.

Table 2. Properties of the Polymer Affecting Stability in Flash Nanoprecipitation

hydrophobic block	PS	PCL	PLA	PLGA
noncrystallizable	Y	N	Y	Y
$T_g > T_{room}$	Y	N	Y	Y
$\lVert\Delta\delta_{PEG}\rvert \gg 0$	Y	Y	N	Y
stable	Y	N	N	Y
biodegradable	N	Y	Y	Y

Table 3. cLogP Values of Various Hydrophobic Compounds and Stability of Nanoparticles Loaded with Those Agents

molecule	clogP[a]	stable
hydrocortisone	1.62	N
curcumin	3.40	N
triiodophenol	4.82	N
paclitaxel	4.95	N
tetra-*n*-butyl silicate	5.92	Y
betulin	6.28	N
2′-triethoxy-PTX-Si	6.56	Y
2′-tri-*i*-propoxy-PTX-Si	7.65	Y
2′,7-bis(triethoxy)-PTX-Si	7.81	Y
2′-di-*tert*-butoxyethoxy-PTX-Si	8.69	Y
2′,7-bis(tri-*i*-propoxy)-PTX-Si	9.21	Y
β-carotene	9.84	Y
tetramenthyl silicate	10.05	Y
2′-trioctyloxy-PTX-Si	10.19	Y
2′-trimenthoxy-PTX-Si	10.24	Y
2′,7-bis(trioctyloxy)-PTX-Si	10.99	Y

[a]cLogP as calculated by molinspiration [www.molinspiration.com].

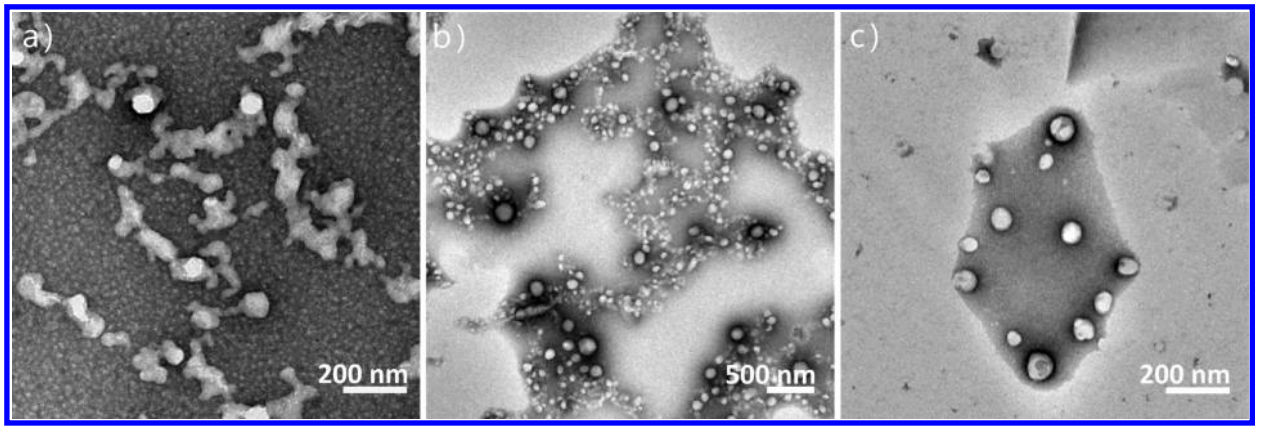

Figure 3. TEM images of (a) 5k−5k PEG-*b*-PLA, (b) 5k−10k PEG-*b*-PLGA, and (c) 10k−10k PEG-*b*-PLGA particles. All particles were made using β-carotene as the hydrophobic small molecule at 50 wt %.

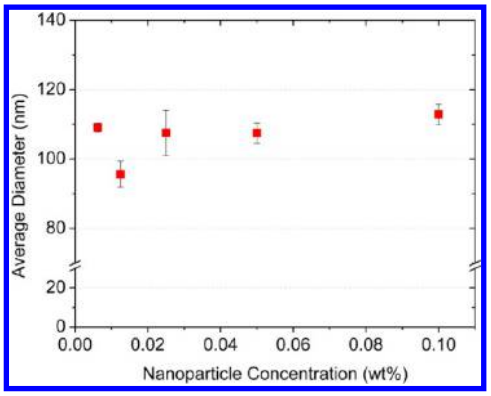

Figure 4. Effect of solute concentration on nanoparticle size. All particles were prepared using 5k−10k PEG-*b*-PLGA and tetramenthyl silicate [$(MenO)_4Si$] at equal mass ratio.

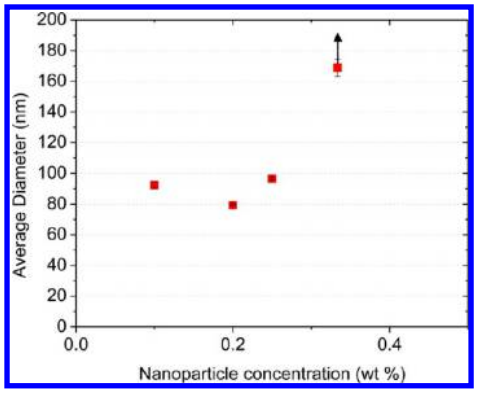

Figure 5. Effect of final dilution on nanoparticle size (hydrodynamic diameter) and stability. All particles were made using 5k−10k PEG-*b*-PLGA and *β*-carotene.

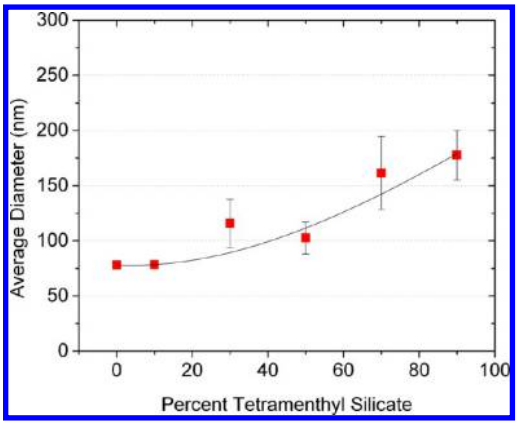

Figure 6. Effect of loading level on nanoparticle size in FNP. All particles were made using 5k−10k PEG-*b*-PLGA and $(MenO)_4Si$. The ratio of polymer to $(MenO)_4Si$ was varied while the total solute concentration was kept constant at 0.1 wt %.

stabilized. Thus, stability is defined as the particles having no noticeable change in size (as judged by DLS measurements). The 5k−10k PEG-*b*-PS BCP gave rise to particles that were stable for at least 10 days. Previous studies also report good stability using PEG-*b*-PS in FNP.[13,18,20,22,24] However, PEG-*b*-PS is nondegradable. Therefore, a series of degradable polyesters—namely, PEG-*b*-PCL, PEG-*b*-PLA, and PEG-*b*-PLGA—was also investigated for their ability to provide stable nanoparticles.

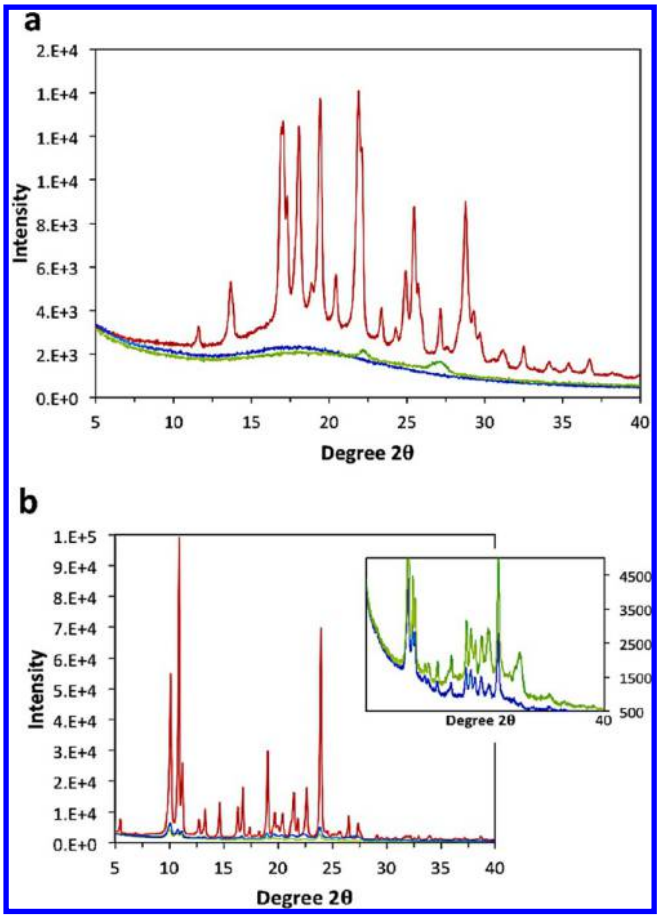

Figure 7. X-ray diffraction (XRD) of (a) *β*-carotene and (b) tetramenthyl silicate ($(MenO)_4Si$) as the pure compound (red) vs nanoparticles (5k−10k mPEG-*b*-PLGA BCP) loaded with 90 wt % (blue) and 50 wt % (green) $(MenO)_4Si$. The inset with expanded scale clearly shows the $(MenO)_4Si$ remains crystalline in the 90 wt % and 50 wt % nanoparticles.

Table 4. Relative Intensities of ^1H NMR Resonances for Various Portions of the Backbone of a PEG-*b*-PLGA BCP (5k−5k) Measured in d_6-Acetone Containing Increasing Amounts of D_2O

method of NMR sample preparation	% D_2O[a]	PEG backbone integration (%)[b]	glycolyl integration (%)[b]	lactyl integration (%)[b]
A[c]	0	100	100	100
A	20	99.5	82.1	96.1
A	33	98.9	65.9[d]	92.8[d]
A	50	95.7	17.9[d]	48.8[d]
A	75	99.6	n.o.[e]	n.o.
A	90	94.2	n.o	n.o.
B[f]	0	100	100	100
B	90	88.5	n.o.	n.o.

[a]Volume of D_2O as a percent of the total volume of solvent (D_2O and d_6-acetone). [b]Methanol was used as an internal standard and is miscible at all solvent compositions. The integrated intensity of the resonances for each portion of the BCP backbone was measured vs that of CH_3OH and divided by the value observed for the same resonance in the initial homogeneous solution of 100% d_6-acetone. [c]Method A: slow addition of each new increment of the antisolvent (water). [d]These resonances were very broad. [e]n.o. = not observed. [f]Method B: prepared by FNP (CIJ-D mixer).

dx.doi.org/10.1021/mp400337f | *Mol. Pharmaceutics* 2013, 10, 4367−4377

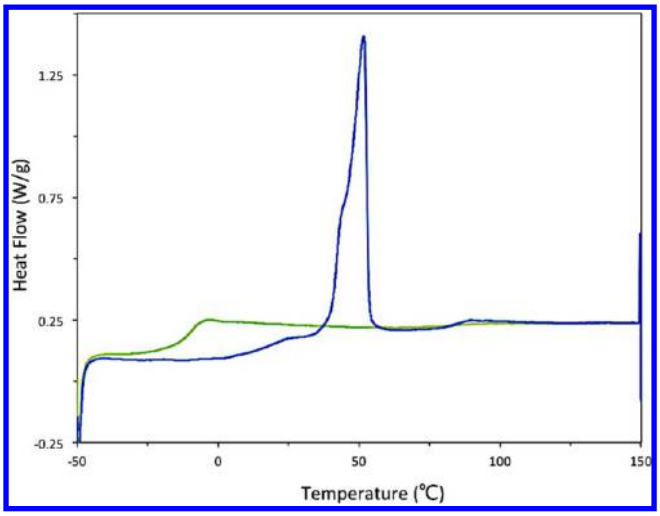

Figure 8. The DSC trace of the FNP-precipitated and freeze-dried 5k−10k PEG-*b*-PLGA BCP shows a strong PEG T_m on the "first run" (blue) indicative of significant phase segregation of the kinetically trapped nanoparticle. A single T_g on the "second run" (green) is characteristic of a phase mixed state at equilibrium.

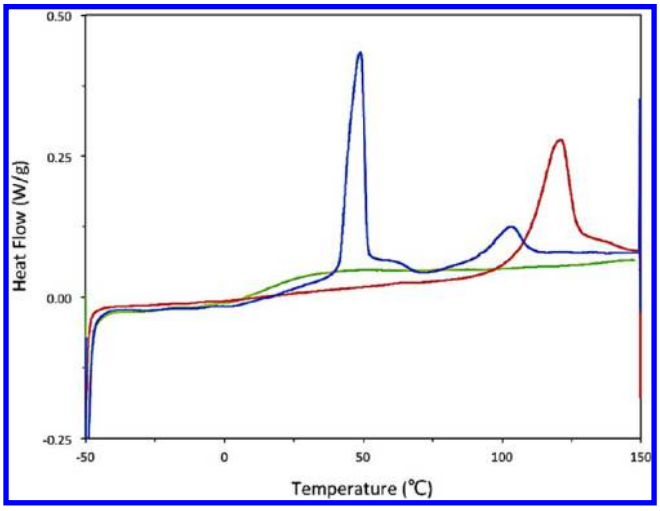

Figure 9. The DSC trace of the FNP-precipitated and freeze-dried nanoparticle composed of equal mass of 2′,7-bis(triethoxy)-PTX-Si and 5k−10k PEG-*b*-PLGA BCP shows a strong PEG T_m and a broad melting point attributed to a depressed melting of the PTX silicate on the "first run" (blue) and a single T_g associated with a phase mixed film in the "second run" (green). The pure 2′,7-bis(triethoxy)-PTX-Si (red) is overlaid on the DSC trace showing a higher T_m and sharper melting transition.

PEG-*b*-PCL has been widely used as a drug delivery system.[8,37,38] However, Zhu showed that particles made using PEG-*b*-PCL were stable for only a few hours in suspension with nanoparticle morphology changing from spherical to irregular shape.[18] Budijuno et al. observed similar problems with PEG-*b*-PCL stabilized particles produced by FNP.[29] The likely cause of the instability is that PCL has a low glass transition temperature (T_g = −60 °C) and therefore relies on crystallization to solidify. Crystallization may not be fast enough to prevent particle coalescence. It may also be slowed by the presence of the drug. PEG-*b*-PCL appears to be a poor choice for stabilization of nanoparticles via FNP.

PLA is known to be biodegradable and biocompatible and is an amorphous polymer with a T_g above room temperature.[39,40] However, *β*-carotene loaded nanoparticles prepared from PEG-*b*-PLA tended to show limited stability. While they appeared to be stable for at least 24 h, precipitation and aggregation occurred over longer periods of time. Moreover, when 1 wt % of NaCl was added, the nanoparticle suspension sedimented within a few hours. These observations as well as those of Zhu[18] indicated that particles were not well stabilized by PEG-*b*-PLA.,

Although particles made by FNP are kinetically trapped far from equilibrium, we expect that thermodynamic driving forces will have an influence. Table 1 gives the glass transition temperatures and solubility parameters in water for each of the polymer blocks ($\delta_{polymer}$) used in these studies, and from these parameters the difference between each hydrophobic block with PEG was calculated as $|\Delta\delta_{PEG}|$. A smaller $|\Delta\delta_{PEG}|$ indicates a greater compatibility with PEG.[41] PLA and PEG have relatively close values for their solubility parameters, resulting in a small value of $|\Delta\delta_{PEG}|$. As a result some PEG may be trapped with PLA in the core of nanoparticles, leading to less surface coverage by PEG and, therefore, less protection. In contrast to these results Prud'homme and co-workers[17,25,28,42] have found PEG-*b*-PLA-protected particles to be stable. However, they either dialyzed or lyophilized and redispersed their particles to remove THF. Since we did not remove THF, PLA may have better solubility in our water/THF medium, resulting in the lower stability that we observed. It is also useful to note that, based on its solubility parameter, *β*-carotene is expected to be highly insoluble in PEG, PLA, and PLGA as can be seen in the $|\Delta\delta_{\beta}|$ calculations shown in Table 1.

Use of PEG-*b*-PLGA as the BCP resulted in spherical nanoparticles, as shown in Figure 3, that were stable in suspension for at least 10 days. Like PLA, PLGA is also a biodegradable, biocompatible, amorphous polymer with a T_g above room temperature. However, it has a larger difference in solubility with PEG than PLA and a slightly higher T_g. We would therefore expect less PEG to be trapped in the core of a PEG-*b*-PLGA-based nanoparticle, resulting in higher surface coverage and greater stability.

To further compare PEG-*b*-PLA with PEG-*b*-PLGA, nanoparticles made from BCP of varying block sizes were made using the CIJ-D mixer and equal mass of BCP and *β*-carotene. When particles were negatively stained with uranyl acetate and viewed with TEM, differences in morphology were observed as shown in Figure 3. The 5k−5k PEG-*b*-PLA particles were often fused. We speculate that the PEG-*b*-PLA particles were partially electrostatically stabilized. Addition of uranyl acetate neutralized the surface charge, triggering aggregation of the PEG-*b*-PLA nanoparticles. The PEG-*b*-PLGA particles did not exhibit this type of behavior: particles appeared to be spherical in morphology.

Polymer properties affecting the stability of *β*-carotene loaded nanoparticles in FNP are summarized in Table 2. Our results suggest that the hydrophobic block of the BCP should be amorphous, have a T_g higher than usage temperature, and a $|\Delta\delta_{PEG}| \gg 0$. Additionally, the polymer should be biocompatible and biodegradable. Based on these criteria, PEG-*b*-PLGA appears to have the best properties for stabilization of nanoparticles made by FNP.

Different molecular weight BCPs of PEG-*b*-PLGA were employed to determine its effect on particle size.[18] Particles were made with equal mass of BCP and *β*-carotene in THF using the MIV mixer. In each case, the average diameter did not show a significant change in size. Addition of 1 wt % saline did

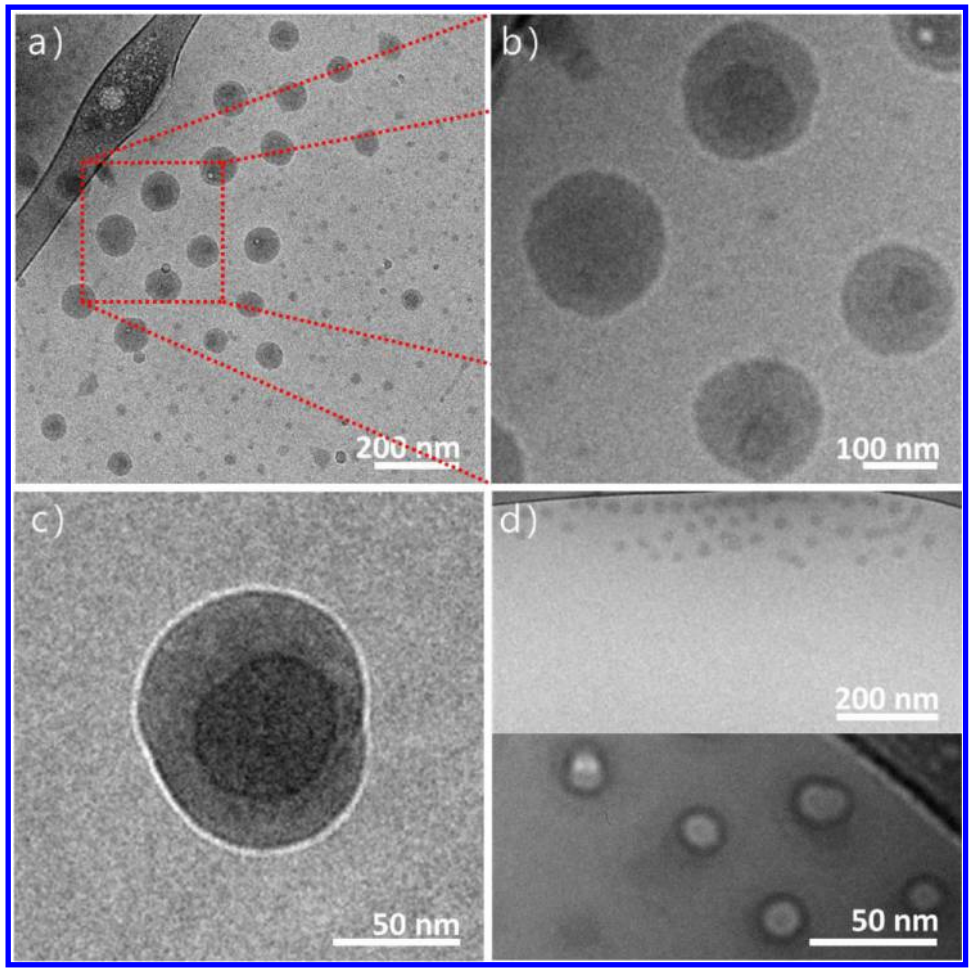

Figure 10. Cryo-TEM micrographs of nanoparticles loaded with 2′,7-bis(triethoxy)-PTX silicate. (a) A low magnification image showing spherical NPs and their size distribution. (b) A higher magnification image of a portion of that field showing core−shell features. (c) An underfocused image that emphasizes the core−shell nature of one particle. (d) Polymer only particles prepared the same way but without the PTX silicate. DLS gave similar size, 30−40 nm.

not lead to an increase in particle size, showing that the particles were sterically stabilized. β-Carotene particles were also made using the CIJ-D mixer at 50 wt % of 5k−10k or 10k−10k PEG-*b*-PLGA. Both were stable, 100 nm hydrodynamic diameter particles. Therefore, PEG-*b*-PLGA BCP was chosen to prepare particles for all subsequent studies.

3.2. Effect of Solute Solubility. The goal of FNP is to formulate hydrophobic small molecules into nanosize delivery vehicles, preferably at high loading levels. Paclitaxel is an example of a drug whose delivery is hindered by its hydrophobicity. Zhu made paclitaxel-loaded nanoparticles by FNP using the two stream CIJ-D mixer and 50 wt % of 2k−10k PEG-*b*-PLGA as the stabilizing BCP.[18] Nanoparticles in the 100−200 nm size range formed initially, but were not stable over the course of 24 h. The particles underwent fast Ostwald ripening and recrystallization. Paclitaxel is too highly hydrophobic to have significant concentration in aqueous medium, but too hydrophilic to be efficiently encapsulated and stabilized in nanoparticle cores at 50% loading.

Solubility therefore plays an important role in nanoparticle stability. For a given hydrophobic compound, the solubility at a specific temperature can be decreased by (1) decreasing the ratio of organic solvent to water, (2) choosing a relatively poor organic solvent, or (3) chemical modification of the compound, to give rise to a more hydrophobic derivative. We describe here examples of the last of these three approaches. Conjugation of silicate esters to paclitaxel can be used to form a more hydrophobic derivative.[35] During administration, the paclitaxel silicate may undergo hydrolysis back to its active form *in vivo*. By covalently bonding a triethoxy silyl moiety to the hydroxyl groups at the C7 and C2′ positions on paclitaxel, a more hydrophobic derivative was made that could be used to make particles that were stable in suspension over a period of several days (see Table 3). The extent to which the hydrophobic small molecule is soluble in water, as judged by, e.g., its logP value (below), should be a good indication of whether or not stable, highly loaded nanoparticles can be formed by FNP.

In order to better understand the effect of drug solubility on nanoparticle stability, a variety of hydrophobic small molecules were used in FNP, including several paclitaxel silicate derivatives. All particles were made using equal mass of drug and PEG-*b*-PLGA dissolved in THF. Particle concentration was 0.1 wt % after FNP. Their stability was then correlated to a calculated value for clogP, the octanol−water partition coefficient. Table 3 shows the calculated clogP values as well as whether or not particles were stable. We defined stability here as <20% diameter change over 1 day in 1 wt % saline. Table 3 shows that molecules with clogP values under 6 were unstable, while those with values above 7 were stable. The work of Prud'homme and co-workers on molecules such as

dx.doi.org/10.1021/mp400337f | *Mol. Pharmaceutics* 2013, 10, 4367−4377

bifenthrin, cinnarizine, clozapine, and α-lipoic acid agrees with these trends.[17,22] Thus, clogP gives a good indication of whether or not a given hydrophobic molecule will make stable particles by FNP. It is important to note, however, that drug crystallinity also has an impact on nanoparticle stability.[17]

3.3. Solute Concentration. We studied the effect of solute concentration in the initial organic phase on the resulting nanoparticle size and stability. In solvent exchange precipitations, such as FNP, where a dissolved solute is added to a large volume of nonsolvent, the supersaturation (S) is given by eq 1.

$$S = \frac{c}{c_\infty} \tag{1}$$

Here, c is the total mass of the solute divided by the final solution volume and c_∞ is the bulk solubility in the final solvent mixture.[48] In previous studies, Mahajan and Kirwan explored the nucleation and growth kinetics of lovastatin at low and high supersaturations in the absence of mixing limitations by using a grid mixer with a mixing time of 3 ms.[49] They found that the nucleation rate increased with increasing supersaturation. In addition, both the nucleation rate and growth rate underwent a distinct transition as supersaturation was increased. This transition corresponded to a transition from heterogeneous to homogeneous nucleation. With a high supersaturation, secondary nucleation was largely avoided and the formation of nuclei was favored prior to significant growth. Therefore, a change in the supersaturation should have an effect on the size of nanoparticles in FNP, i.e., with higher supersaturation, more nucleation sites would be generated, which should lead to the formation of smaller nanoparticles.

In the presence of added block copolymers, the hydrophobic molecule should still likely nucleate with itself and have a higher nucleation rate than the block copolymer. The water-soluble PEG block on the copolymer will slow the nucleation of the hydrophobic block. After some growth of small molecule particles the copolymers will assemble on the surfaces of the particles and arrest their growth.

To test these ideas, we examined particles made using tetramenthyl silicate, $(MenO)_4Si$.[35] Like β-carotene, $(MenO)_4Si$ is highly hydrophobic (see Table 3). $(MenO)_4Si$ was dissolved in THF at equal mass ratio with 5k−10k PEG-*b*-PLGA. As shown in Figure 4, altering the solute concentration in the organic solvent by 20-fold had no effect on the size and stability of the $(MenO)_4Si$ loaded nanoparticles. This could be because the degree of supersaturation is so high that nucleation is very fast regardless of the solute concentration in the feed solution. We could not increase the concentration of $(MenO)_4Si$ further due to its maximum solubility in THF. When we decreased nanoparticle concentration below 0.005 wt %, we ran into detection limits of DLS.

A method to decrease supersaturation is to reduce the amount of nonsolvent, i.e., water. In order to produce stable nanoparticles with the CIJ-D mixer, a final dilution is required after mixing (see Figure 1). Han et al.[16] showed that a 5-fold dilution was required to produce *pure β-carotene* particles with diameter <100 nm. The effect of dilution volume with *copolymer-stabilized* particles has not been previously reported. Concentration in the final suspension was therefore varied by altering the final dilution volume in FNP. Particles were made using an equal mass ratio of β-carotene and 5k−10k PEG-*b*-PLGA in THF. Particles made at 0.1 to 0.25 wt % solids were all relatively similar in size, as shown in Figure 5. At 0.35 wt % particle size increased, but stability was reduced. We attempted to produce nanoparticles at a final concentration of 1 wt % solids in the suspension, but nanoparticles grew rapidly in size and precipitated after mixing. Therefore, controlling nanoparticle size beyond ∼0.3 wt % by changing the final dilution volume could not be realized for the materials tested.

3.4. Effect of Loading on Nanoparticle Size. One advantage of using the FNP process to make BCP protected nanoparticles is the ability to make particles with a high loading of the cargo of interest. The theoretical loading level is the ratio (w/w) of the mass of the drug to that of the drug plus the BCP that was introduced in the THF stream during FNP. To better understand how loading affects nanoparticle stability, particles were made with varying loadings of $(MenO)_4Si$, while the total concentration of dissolved solute was kept constant at 0.05 wt % in the final suspension. Particle size increased from about 75 nm with no $(MenO)_4Si$ to 200 nm at 90% $(MenO)_4Si$ loading, as shown in Figure 6. These particles were stable for 1 week in suspension, as well as in 1 wt % saline solution. These results also show that varying the loading levels provides a means to control particle size. However, particles made using β-carotene at 90% loading were not stable in a saline solution. While both molecules have similar calculated clogP values, they differ in morphology inside the core of the nanoparticle. Figure 7 (XRD) shows that $(MenO)_4Si$ in nanoparticles is crystalline whereas β-carotene in nanoparticles is amorphous, which may cause poor stability of the latter.

3.5. Nanoparticle Structure. While we have shown that FNP can be used to make nanoparticles from a variety of compounds provided they are of sufficiently high hydrophobicity, the internal structure of the particles is not known. Improved understanding of the nanoparticle structure is important, because it will certainly affect drug release. For example, a loaded drug may release from the particles more quickly if the particle has a loosely packed structure with some hydrophilic blocks incorporated into the core vs a tightly packed core shell structure. Therefore, we undertook studies to better understand the structure of these nanoparticles.

3.5.1. NMR Studies. NMR spectroscopic techniques are one of many options that provide insight into block copolymer self-assembly and micellization.[37] Davis and co-workers have extensively analyzed the behavior of nanoparticles fabricated from PEG-*b*-PLA BCPs of various MWs via ^{1}H NMR spectroscopy and correlated it with particle sizes obtained by DLS.[50] Briefly, they deduced that the precipitation/evaporation technique they employed resulted in particles with a core−shell structure. They observed large PLA resonances (as judged relative to an internal standard) for low MW polyester blocks (<3k). They interpreted this result as significant polymer mobility at low MWs. In contrast to this finding, analogous resonances were not observed for BCPs with a PLA block size of MW >6k. Additionally, quantitative integration of the PEG block suggested minimal penetration of the PEG chains into the micelle core, indicative of a solid-like PLA core.[50,51]

One key difference between the work in the Davis studies and FNP produced nanoparticles is that precipitation in FNP is potentially much faster, which could lead to kinetically trapped BCP. PEG entrapment within the core, extraneous PLGA corona material, or mobile PLGA chains within the core remain reasonable propositions. It has been shown that the physical state of the polyester block affects drug release.[52]

The initial experiment was similar to the Davis study: a 5k−5k PEG-*b*-PLGA BCP was dissolved in d_6-acetone alone with

methanol as an internal standard. D_2O was progressively titrated into the solution, and the proton NMR resonances attributable to the ethylene oxide, lactic, and glycolic repeat units were integrated. With the progressive addition of D_2O, the PLGA resonances broadened significantly during the experiment, becoming unrecognizable at >50 vol% D_2O content. In contrast, the PEG-related proton resonance remained sharp, and its integration value remained essentially constant throughout the experiment. These results were compared to NMR on particles formed rapidly by FNP using the same solvents and same PEG-*b*-PLGA. The results were essentially the same, as shown in Table 4. After precipitation via FNP, the PLGA resonances were broadened such that they were indistinguishable from the baseline, whereas the PEG resonances remained well-defined and integrated to 88.5% of the value in d_6-acetone. These results are consistent with a solubilized PEG corona and a solid-like PLGA core.

Diffusion oriented spectroscopy (DOSY) was used to provide additional insight about whether the silicate esters were efficiently encapsulated within the BCP nanoparticles.[53,54] Tetra-*n*-butyl silicate, a liquid silicate ester, was chosen as the model compound for these studies because it is liquid (at ambient temperature) and exhibited distinctive ^{1}H resonances that were easily discernible from the BCP resonances after FNP formulation.[35] Thus, the tetra-*n*-butyl silicate was subjected to FNP in the CIJ-D mixer. Equal mass of PEG-*b*-PLGA (5k−10k) and the silicate were dissolved in 2.5 mL of d_6-acetone and then flash precipitated with 2.5 mL of D_2O followed by dilution in 45 mL of D_2O. The dispersion was then analyzed by ^{1}H NMR spectroscopy and compared to the resonance shifts of the silicate dissolved in a d_6-acetone solution and D_2O in the same concentration and solvent ratio.[35] Monomethoxy diethylene glycol was added to both suspensions as a water-soluble, small molecule standard to allow comparison of the diffusion coefficients. The presumably BCP-encapsulated silicate and the soluble monomethoxy diethylene glycol produced a ΔD of $\sim 10^6$ m^2 s^{-1} whereas a ΔD of only $\sim 10^2$ m^2 s^{-1} was observed for the dissolved and simply mixed silicate. This large difference (10^4 m^2 s^{-1}) is consistent with incorporation of the tetraalkyl silicate into the much larger (and more slowly diffusing) nanoparticles. Moreover, the fact that we can observe the silicate protons as reasonably sharp resonances suggests that it is not embedded in the PLGA blocks but rather resides in its own separate mobile liquid phase inside the nanoparticle, nor is the tetra-*n*-butyl silicate likely to reside in emulsion droplets based on the ∼200 nm particle size and particle stability.

Evidence for high encapsulation was also demonstrated for a silicate derivative loaded particle. 2′,7-Bis(triethoxy)-PTX-Si particles were flash precipitated with an equal mass of PEG-*b*-PLGA (5k−10k). Control particles were made without using any stabilizing PEG-*b*-PLGA. The particles were freeze-dried following FNP and then redispersed in water. Diethyl ether, a good solvent for the silicate but not for PEG or the BCP, was then used to extract each of these two aqueous dispersions. The content of the ether extract was analyzed by ^{1}H NMR spectroscopy. Without block copolymer protection, >85% of the silicate derivative was recovered, while with PEG-*b*-PLGA protection, the particles only lost 7% of their silicate content even after multiple extractive washings with ether. This result also demonstrates that >90% of the silicate was encapsulated in the nanoparticle core.

3.5.2. Differential Scanning Calorimetry. The structure and morphology of nanoparticles (freeze-dried, 5k−10k PEG-*b*-PLGA nanoparticles made using the CIJ-D mixer) was evaluated using DSC. Typically, DSC studies of polymers utilize the "second run" of the trace so that the measured properties are independent of the polymer's thermal history. In the case of the FNP-produced polymers, however, data from the "first run" are instructive. The "first run" DSC trace of unloaded PEG-*b*-PLGA nanoparticles exhibited a strong T_m of the crystalline PEG block at ∼50 °C as shown in Figure 8. This is a depressed melting transition temperature relative to the pure PEG homopolymer (which exhibited a T_m of ∼60 °C in a control experiment). This observation is consistent with incomplete phase segregation. The T_g from the PLGA block was not obvious in the trace, but it is conceivable that there is a weak, broad glass transition at ∼20 °C whereas the T_g of pure PLGA is 39 °C (see Table 1). This observation is consistent with some polyether/polyester mixing.[55]

Recrystallization of the PEG did not occur upon cooling, and the "second run" DSC trace exhibited a single T_g. This result was reproduced when the polymer was cooled at an exceedingly slow rate (1 °C·s^{-1}), consistent with a thermodynamically stable, phase-mixed system. Based on these results, a reasonable conclusion is that the polymer blocks are largely, but not exclusively, phase-segregated following FNP and lyophilization. This further supports the core−shell structure of these nanoparticles.

With a basic understanding of the DSC behavior of the precipitated polymer, we turned our attention to the analysis of a paclitaxel silicate [2′,7-bis(triethox)-PTX-Si] loaded nanoparticle. Particles were made using an equal mass of BCP and the silicate in the CIJ-D mixer and were lyophilized immediately after nanoprecipitation. Again, a strong, depressed PEG T_m at ∼50 °C was evident (Figure 9). Additionally, there was a broad melting point centered at ∼105 °C. This endothermic peak occurs at a lower temperature and is broader than that for the pure PTX silicate (red curve in Figure 9) indicating an impure, crystalline melting transition of the PTX silicate. After cooling, a single T_g was again noted during the second heating cycle, a feature consistent with a well-mixed, silicate-loaded polymer film (rather than nanoparticles).

3.5.3. Cryo-TEM. Cryo-TEM was employed to obtain further definition of the nanoscopic structure of these nanoparticles. Particles were prepared using PEG-*b*-PLGA (5k−10k) and 2′,7-bis(triethoxy)-PTX-Si at 50 wt % loading. Figure 10 shows that the particles are predominately spherical in nature. A subset of substantially smaller nanoparticles can also be seen. These smaller particles are perhaps indicative of unloaded, block-copolymer only particles. They are of similar size to particles prepared with only PEG-*b*-PLGA (5k−10k) shown in Figure 10d. The higher resolution micrographs in Figures 10b and 10c confirm the core shell microstructure suggested by the NMR and DSC experiments described above. Figure 10c indicates that the PTX-Si is encapsulated with the solid-like PLGA block of the copolymer, which is in turn surrounded by the soluble corona of the hydrophilic PEG blocks. The PEG corona is not visible here because of its low density.

4. CONCLUSIONS

Our results support a model for FNP proposed by Johnson and Prud'homme.[14] When the organic solution of the hydrophobic compound and diblock copolymer collides with water in the turbulent impingement chamber, the solvent and water quickly mix, creating a supersaturated solution. The hydrophobic compound nucleates and grows, but that growth is arrested by

encapsulation by the hydrophobic block of the BCP. The hydrophilic PEG block remains in solution, where it can stabilize the nanoparticles in the resulting aqueous dispersion. We suggest a three-layer structure in which the loaded nanoparticles consist of a core rich in the small molecule, surrounded by a shell of PLGA and a corona of PEG.

The cryoTEM images in Figure 10 with their spherical cores are most supportive of this model. The PEG corona is not visible as it is likely swollen with vitrified water and has low electron density. The first run DSC results in Figure 9 also support a three-layer model. The crystal melting peaks for both PEG and the silicate derivative indicate that they are phase separated. Their melting peaks are depressed due to rapid precipitation and perhaps some phase mixing. However, if the silicate were well mixed with PLGA it would likely not be able to crystallize at all. The NMR results show that, for particles made only with PEG-*b*-PLGA, PEG is in the corona and PLGA is immobilized. When tetra-*n*-butyl silicate was added, DOSY NMR showed that it remained liquid, indicating that the silicate was not phase mixed with the PLGA. Extraction with diethyl ether also demonstrated nearly complete encapsulation of 2′,7-triethoxy-PTX-Si.

Our results along with those in the literature suggest the following guidelines for synthesis of 100 nm particles with ≥50% loading of drug by FNP.

1. The small molecule candidate for FNP should have clogP < 6 and >1% solubility in a water miscible solvent. Acetone is an attractive water miscible solvent for pharmaceutical applications.
2. An amphiphilic diblock copolymer is required to stabilize particles. PEG of 5000 molecular weight seems the best choice for the hydrophilic block. The hydrophobic block should be biodegradable with T_g > 37 °C and low solubility with PEG. PLGA performed best in our studies, but changing the molecular weight between 5 and 15k did not affect particle size.
3. Nanoparticle formation requires intense mixing, i.e., high Reynolds number, which is defined as the ratio of inertial to viscous forces. We always used Re > 3000. Other studies have shown that Re ≥ 3000 produces minimum particle diameter.[16,56]
4. At equal mass ratio of small molecule to copolymer particle size is ∼100 nm independent of total solids concentration over the range 0.005−0.3 wt %. At higher concentrations size increased but particles became unstable.
5. It is possible to create particles loaded with 90% of highly insoluble small molecules, clogP ∼10. Size increases to 200 nm at this loading. If such insoluble molecules are crystallizable, they may be more stable at high loading.

AUTHOR INFORMATION

Corresponding Author

*E-mail: macosko@umn.edu.

Present Address

A.R.W.: HB Fuller, Minneapolis, MN.

Notes

The authors declare no competing financial interest.

ACKNOWLEDGMENTS

We would like to acknowledge financial support from the University of Minnesota Futures Grant Program and the National Institutes of Health (EB011671). Yuqiang Qian obtained the xrd data. Parts of this work were carried out in the Characterization Facility, University of Minnesota, a member of the NSF-funded Materials Research Facilities Network (www.mrfn.org) via the MRSEC program. A.R.W. thanks the 3M Corporation for providing a 3M Science and Technology Fellowship.

REFERENCES

(1) Lipinski, C. Poor Aquous Solubility—An Industry Wide Problem in Drug Discovery. *Am. Pharm. Rev.* **2002**, *5*, 82−85.

(2) Goldberg, M.; Langer, R.; Jia, X. Nanostructured Materials for Applications in Drug Delivery and Tissue Engineering. *J. Biomater. Sci., Polym. Ed.* **2007**, *18*, 241−68.

(3) Brannon-Peppas, L.; Blanchette, J. O. Nanoparticle and Targeted Systems for Cancer Therapy. *Adv. Drug Delivery Rev.* **2004**, *56*, 1649−59.

(4) Matsumura, Y.; Maeda, H. A New Concept for Macromolecular Therapeutics in Cancer Chemotheray: Mechanism of Tumor Tropic Accumulation of Proteins and Antitumor Agent SMANCS. *Cancer Res.* **1986**, *46*, 6387−6392.

(5) Kim, S. Liposomes as Carriers of Cancer Chemotherapy—Current Status and Future Prospects. *Drugs* **1993**, *46*, 618−638.

(6) Discher, D. E.; Eisenberg, A. Polymer Vesicles. *Science (New York, N.Y.)* **2002**, *297*, 967−73.

(7) Kwon, G. Diblock Copolymer Nanoparticles for Drug Delivery. *Crit. Rev. Ther. Drug Carrier Syst.* **1998**, *15*, 481−512.

(8) Allen, C. Nano-engineering Block Copolymer Aggregates for Drug Delivery. *Colloids Surf., B* **1999**, *16*, 3−27.

(9) Ahmed, F.; Pakunlu, R. I.; Brannan, A.; Bates, F.; Minko, T.; Discher, D. E. Biodegradable Polymersomes Loaded with Both Paclitaxel and Doxorubicin Permeate and Shrink Tumors, Inducing Apoptosis in Proportion to Accumulated Drug. *J. Controlled Release* **2006**, *116*, 150−8.

(10) Ghoroghchian, P. P.; Lin, J. J.; Brannan, A. K.; Frail, P. R.; Bates, F. S.; Therien, M. J.; Hammer, D. a. Quantitative Membrane Loading of Polymer Vesicles. *Soft Matter* **2006**, *2*, 973.

(11) Kataoka, K.; Matsumoto, T.; Yokoyama, M.; Okano, T. Doxorubicin-loaded Poly(ethylene Glycol)-polu(beta-benzyl-l-apspartate) Copolymer Micelles: Their Pharmaceutical Characteristics and Biological Significance. *J. Controlled Release* **2000**, *64*, 143−153.

(12) Gelderblom, H.; Verweij, J.; Nooter, K.; Sparreboom, A.; Cremophor, E. L. The Drawbacks and Advantages of Vehicle Selection for Drug Formulation. *Eur. J. Cancer* **2001**, *37*, 1590−1598.

(13) Johnson, B. K.; Prud'homme, R. K. Chemical Processing and Micromixing in Confined Impinging Jets. *AIChE J.* **2003**, *49*, 2264−2282.

(14) Johnson, B. K.; Prud'homme, R. K. Flash Nanoprecipitation of Organic Actives and Block Copolymers Using a Confined Impinging Jets Mixer. *Aust. J. Chem.* **2003**, *56*, 1021.

(15) Gindy, M. E.; Panagiotopoulos, A. Z.; Prud'homme, R. K. Composite Block Copolymer Stabilized Nanoparticles: Simultaneous Encapsulation of Organic Actives and Inorganic Nanostructures. *Langmuir* **2008**, *24*, 83−90.

(16) Han, J.; Zhu, Z.; Qian, H.; Wohl, A. R.; Beaman, C. J.; Hoye, T. R.; Macosko, C. W. A Simple Confined Impingement Jets Mixer for Flash Nanoprecipitation. *J. Pharm. Sci.* **2012**, *101*, 4018−4023.

(17) Pinkerton, N.; Grandeury, A.; Fisch, A.; Brozio, J.; Riebesehl, B.; Prud'homme, R. Formation of Stable Nanocarriers by in Situ Ion Pairing During Block-copolymer-directed Rapid Precipitation. *Mol. Pharmaceutics* **2013**, *10*, 319−328.

(18) Zhu, Z. Polymer Stabilized Nanosuspensions Formed via Flash Nanoprecipitation: Nanoparticle Formation, Formulation, and Stability, Ph.D. Thesis, University of Minnesota, Minneapolis, MN, 2010.

(19) Gindy, M. E.; Ji, S.; Hoye, T. R.; Panagiotopoulos, A. Z.; Prud'homme, R. K. Preparation of Poly(ethylene Glycol) Protected Nanoparticles with Variable Bioconjugate Ligand Density. *Biomacromolecules* **2008**, *9*, 2705−11.

(20) Shen, H.; Hong, S.; Prud'homme, R. K.; Liu, Y. Self-assembling Process of Flash Nanoprecipitation in a Multi-inlet Vortex Mixer to Produce Drug-loaded Polymeric Nanoparticles. *J. Nanopart. Res.* **2011**, *13*, 4109−4120.
(21) Akbulut, M.; Ginart, P.; Gindy, M. E.; Theriault, C.; Chin, K. H.; Soboyejo, W.; Prud'homme, R. K. Generic Method of Preparing Multifunctional Fluorescent Nanoparticles Using Flash NanoPrecipitation. *Adv. Funct. Mater.* **2009**, *19*, 718−725.
(22) Liu, Y.; Tong, Z.; Prud'homme, R. K. Stabilized Polymeric Nanoparticles for Controlled and Efficient Release of Bifenthrin. *Spectrum* **2008**, *812*, 808−812.
(23) Kumar, V.; Prud'homme, R. K. Nanoparticle Stability: Processing Pathways for Solvent Removal. *Chem. Eng. Sci.* **2009**, *64*, 1358−1361.
(24) Ansell, S. M.; Johnstone, S. A.; Tardi, P. G.; Lo, L.; Xie, S.; Shu, Y.; Harasym, T. O.; Harasym, N. L.; Willaims, L.; Bermudes, D.; et al. Modulating the Therapeutic Activty of Nanoparticle Delivered Paclitaxel by Manipulating the Hydrophobicity of Prodrug Conjugates. *J. Med. Chem.* **2008**, *51*, 3288−3296.
(25) D'Addio, S. M.; Saad, W.; Ansell, S. M.; Squiers, J. J.; Adamson, D. H.; Herrera-Alonso, M.; Wohl, A. R.; Hoye, Thomas, R.; Macosko, C. W.; Mayer, L. D. Effects of Block Copolymer Properties on Nanocarrier Protection from in Vivo Clearance. *J. Controlled Release* **2012**, *162*, 208−217.
(26) Liu, Y.; Kathan, K.; Saad, W.; Prud'homme, R. K. Ostwald Ripening of Beta-carotene Nanoparticles. *Phys. Rev. Lett.* **2007**, *98*, 036102.
(27) D'Addio, S. M.; Kafka, C.; Akbulut, M.; Beattie, P.; Saad, W.; Herrera, M.; Kennedy, M. T.; Prud, R. K. Novel Method for Concentrating and Drying Polymeric Nanoparticles: Hydrogen Bonding Coacervate Precipitation. *Mol. Pharmaceutics* **2010**, *7*, 557−564.
(28) Kumar, V.; Hong, S. Y.; Maciag, A. E.; Saavedra, J. E.; Adamson, D. H.; Prud'homme, R. K.; Keefer, L. K.; Chakrapani, H. Stabilization of the Nitric Oxide (NO) Prodrugs and Anticancer Leads, PABA/NO and Double JS-K, Through Incorporation into PEG-protected Nanoparticles. *Mol. Pharmaceutics* **2010**, *7*, 291−298.
(29) Budijono, S. J.; Shan, J.; Yao, N.; Miura, Y.; Hoye, T.; Austin, R. H.; Ju, Y.; Prud'homme, R. K. Synthesis of Stable Block-Copolymer-Protected NaYF 4:Yb 3+, Er 3+ Up-Converting Phosphor Nanoparticles. *Chem. Mater.* **2010**, *22*, 311−318.
(30) Cheng, K. K.; Yeung, C. F.; Ho, S. W.; Chow, S. F.; Chow, A. H. L.; Baum, L. Highly Stabilized Curcumin Nanoparticles Tested in an In Vitro Blood-Brain Barrier Model and in Alzheimer's Disease Tg2576 Mice. *AAPS J.* **2013**, *15* (2), 324−336.
(31) Shi, L.; Shan, J.; Ju, Y.; Aikens, P.; Prud'homme, R. K. Nanoparticles as Delivery Vehicles for Sunscreen Agents. *Colloids Surf., A* **2012**, *396*, 122−129.
(32) Cheng, J. C.; Vigil, R. D.; Fox, R. O. A Competitive Aggregation Model for Flash Nanoprecipitation. *J. Colloid Interface Sci.* **2010**, *351*, 330−42.
(33) Ji, S.; Zhu, Z.; Hoye, T. R.; Macosko, C. W. Maleimide Functionalized Poly(ε-caprolactone)-b-poly(ethylene Glycol) (PCL-PEG-MAL): Synthesis, Nanoparticle Formation, and Thiol Conjugation. *Macromol. Chem. Phys.* **2009**, *210*, 823−831.
(34) Qian, H.; Wohl, A. R.; Crow, J. T.; Macosko, C. W.; Hoye, T. R. A Strategy for Control of "Random" Copolymerization of Lactide and Glycolide: Application to Synthesis of PEG-b-PLGA Block Polymers Having Narrow Dispersity. *Macromolecules* **2011**, *44*, 7132−7140.
(35) Wohl, A. R. Synthesis and Characterization of Silicate Ester Prodrugs and Poly(ethylene Glycol)-b-poly(lactic-co-glycolic Acid) Block Copolymers for Formulation into Prodrug-loaded Nanoparticles, Ph.D. Thesis, University of Minnesota, Minneapolis, MN, 2012.
(36) Grassucci, R. A.; Taylor, D.; Frank, J. Visualization of macromolecular complexes using cryo-electron microscopy with FEI Tecnai transmission electron microscopes. *Nat. Protoc.* **2008**, *3*, 330−339.
(37) Riess, G. Micellization of Block Copolymers. *Prog. Polym. Sci.* **2003**, *28*, 1107−1170.
(38) Torchilin, V. P. Structure and Design of Polymeric Surfactant-based Drug Delivery Systems. *J. Controlled Release* **2001**, *73*, 137−172.
(39) Chaubal, M. Polylactides/glycolides-excipients for Injectable Drug Delivery and Beyond. *Drug Delivery Technol.* **2002**, *2*, 34−36.
(40) Sheftel, V. O. *Indirect Food Additives and Polymers: Migration and Toxicology*; CRC Press, 2000; pp 1114−1116.
(41) Hiemenz, P. C.; Lodge, T. P. *Polymer Chemistry*, 2nd ed.; CRC Press: Boca Raton, Fl, 2007; pp 354−357.
(42) Figueroa, C. E.; Reider, P.; Burckel, P.; Pinkerton, A. A.; Prud'homme, R. K. Highly Loaded Nanoparticulate Formulation of Progesterone for Emergency Traumatic Brain Injury Treatment. *Ther. Delivery* **2012**, *3*, 1269−1279.
(43) Tormala, P. Determination of Glass Transition Temperature of Poly(ethylene Glycol) by Spin Probe Technique. *Eur. Polym. J.* **1974**, *10*, 519−521.
(44) Overney, R. M.; Buenviaje, C.; Luginbuhl, R.; Dinelli, F. Glass and Structural Transition Temperature at Polymer Surfaces on The Nanoscale. *J. Therm. Anal. Calorim.* **2000**, *59*, 205−225.
(45) Izuka, A.; Winter, H. H.; Hashimoto, T. Molecular Weight Dependence of Viscoelasticity of Polycaprolactone Critical Gels. *Macromolecules* **1992**, *25*, 2422−2428.
(46) Omelczuk, M. O.; McGinity, J. W. The Influence of Polymer Glass Transition Temperaute and Molecular Weight on Drug Release from Tablets Containing Poly(dl-lactic Acid). *Pharm. Res.* **1992**, *9*, 26−32.
(47) Houchin, M. L.; Topp, E. M. Physical Properties of PLGA Films During Polymer Degradation. *J. Appl. Polym. Sci.* **2009**, *114*, 2848−2854.
(48) Brick, M. C.; Palmer, H. J.; Whitesides, T. H. Formation of Colloidal Dispersions of Organic Materials in Aqueous Media by Solvent Shifting. *Langmuir* **2003**, *19*, 6367−6380.
(49) Mahajan, A. J.; Kirwan, D. J. Nucleation and Growth Kinetics of Biochemicals Measured at High Supersaturations. *J. Cryst. Growth* **1994**, *144*, 281−290.
(50) Riley, T.; Stolnik, S.; Heald, C. R.; Xiong, C. D.; Garnett, M. C.; Illum, L.; Davis, S. S.; Purkiss, S. C.; Barlow, R. J.; Gellert, P. R. Physicochemical Evaluation of Nanoparticles Assembled from Poly(lactic Acid)-poly(ethylene Glycol) (PLA-PEG) Block Copolymers as Drug Delivery Vehicles. *Langmuir* **2001**, *17*, 3168−3174.
(51) Heald, C. R.; Stolnik, S.; Kujawinski, K. S.; De Matteis, C.; Garnett, M. C.; Illum, L.; Davis, S. S.; Purkiss, S. C.; Barlow, R. J.; Gellert, P. R. Poly(lactic Acid)-poly(ethylene oxide) (PLA-PEG) Nanoparticles: NMR Studies of the Central Solidlike PLA Core and the Liquid PEG Corona. *Langmuir* **2002**, *18*, 3669−3675.
(52) Papadimitriou, S.; Bikiaris, D. Novel Self-assembled Core-shell Nanoparticles Based on Crystalline Amorphous Moieties of Aliphatic Copolyesters for Efficient Controlled Drug Release. *J. Controlled Release* **2009**, *138*, 177−84.
(53) Garcia-Fuentes, M.; Torres, D.; Martín-Pastor, M.; Alonso, M. J. Application of NMR Spectroscopy to the Characterization of PEG-stabilized Lipid Nanoparticles. *Langmuir* **2004**, *20*, 8839−45.
(54) Valentini, M.; Vaccaro, A.; Rehor, A.; Napoli, A.; Hubbell, J. A.; Tirelli, N. Diffusion NMR Spectroscopy for the Characterization of the Size and Interactions of Colloidal Matter: The Case of Vesicles and Nanoparticles. *J. Am. Chem. Soc.* **2004**, *126*, 2142−7.
(55) Kulinski, Z.; Piorkowska, E.; Gadzinowska, K.; Stasiak, M. Plasticization of poly(L-lactide) with Poly(propylene Glycol). *Biomacromolecules* **2006**, *7*, 2128−35.
(56) Liu, Y.; Chen, C.; Prud'homme, R.; Fox, R. Mixing in a Multi-Inlet Vortex Mixer (MIVM) for Flash Nano-Precipitation. *Chem. Eng. Sci.* **2008**, *63*, 2829−42.